Fire Safety Journal 140 (2023) 103918

Contents lists available at ScienceDirect

Fire Safety Journal

journal homepage: www.elsevier.com/locate/firesaf

Flammability and burning behaviour of fire protected timber

Iben Hansen-Bruhn [a,b,c], T. Richard Hull [a,*]

[a] Centre for Fire and Hazard Science, University of Central Lancashire, Preston, PR1 2HE, UK
[b] Plastic and Polymer Engineering, Department of Biological and Chemical Engineering, Aarhus University, Aabogade 40, 8200, Aarhus N., Denmark
[c] Teknos Fire Retardant Technology, R&D, Teknos A/S, Industrivej 19, DK-6580, Vamdrup, Denmark

ARTICLE INFO

Keywords:
Fire chemistry
Heat release rate
Protection of wood
Fire impregnation
Intumescent coatings
Risk assessment

ABSTRACT

Decarbonization has driven the construction industry to rediscover biobased, but inherently combustible, materials like timber. To avoid compromising fire safety, reaction to fire of timber can be effectively reduced by fire retardant surface coatings or impregnation treatments. Using a combination of simultaneous thermal analysis, microscale combustion calorimetry and cone calorimetry, vacuum-pressure impregnated (boron free, phosphorus-based) plywood was tested against plywood coated with a thin layer of water-based fire retardant intumescent coating (melamine free, phosphorus-based). Comparing the peak heat release rate (*pHRR*) and total heat release (*THR*) of the three plywood samples, the impregnated was lowest, and the coated was lower (*pHRR* −34% and −20%, *THR* -45% and −21% respectively) relative to the untreated plywood. In contrast, the coating layer postponed sustained flaming for longer than impregnated wood and delayed burnthrough, effects critical to the growth rate of a developing fire. Better understanding of the assessment of flammability of fire protected timber has been obtained using cone calorimeter data supported by microscale analyses. The results challenge the simple flammability ranking based on total heat release, and highlight the need for further development of a methodology for comparing different fire protection strategies for timber.

1. Introduction

The Food and Agriculture Organization of United Nations (FAO) estimates that the total consumption of wood products by volume, measured in round wood equivalents (RWE), will increase by 35% in 2050 to reach 3.1 billion m^3 RWE [1,2]. This global increase is driven by urbanization, housing demands and decarbonization [3–5]. As a sustainable, adaptable, and readily recyclable material, wood finds its use in a variety of applications. Wood is, however, susceptible to fire. At temperatures above 200–250 °C, wood discolours and chars. Above 300 °C the structure starts to break down. This correlates to the onset of cellulose decomposition that has a maximum mass loss rate around 355 °C [6,7]. Cellulose undergoes complete volatilisation with little char yield, and the vigorous pyrolysis rate of cellulose causes and feeds flaming combustion [8].

The thermal decomposition mechanism of cellulose, first purposed by Shafizadeh in 1979 [9], takes places by two competing mechanisms: 1) dehydration that yields char, carbon monoxide (CO), carbon dioxide (CO_2), and water, 2) depolymerisation that yields tar and combustible volatiles [10]. Dehydration involves scission of ether bonds within the glucose monomer (Fig. 1) resulting in initially stable aliphatic structures, subsequently converted to aromatic structures on sustained heating [11,12]. Depolymerisation is initiated by scission of acetal bonds (Fig. 1) which breaks the polymer backbone leaving reactive ends from which laevoglucosan molecules can form by transglycosylation and volatilise. Laevoglucosan is the main component of tar, and thus flammable gases evolve from the depolymerisation [13]. The balance between the two competitive processes at 300–500 °C (dehydration and depolymerisation) determines the ease of ignition. Numerous studies can be found on thermal degradation and charring of cellulose and wood e.g. Refs. [14,15].

With the construction sector as the main consumer of wood products [2], improvement of fire performance is driven by regulations to ensure fire safety [16]. For passive fire protection of wood, surface- and penetration treatments can be employed:

1) Vacuum-pressure impregnation forces fire retardants into the wood structure. Upon heating, phosphorus-based fire retardants decompose to accelerate char layer formation, thus changing the thermal behaviour and reducing release of flammable volatiles.

* Corresponding author.
E-mail addresses: iben.hansenbruhn@teknos.com (I. Hansen-Bruhn), trhull@uclan.ac.uk (T.R. Hull).

https://doi.org/10.1016/j.firesaf.2023.103918
Received 10 June 2023; Accepted 16 August 2023
Available online 17 August 2023

List of abbreviations

APP	ammonium polyphosphate
CO	Carbon monoxide
CO_2	Carbon dioxide
CC	Cone Calorimetry
FRC	Fire retarded by coating
FRP	Fire retarded by pressure impregnation
MAP	Mono ammonium phosphate
MCC	Microscale Combustion Calorimetry
n	Number of repetitions
PTFE	Polytetrafluoroethylene
RWE	Round wood equivalents
STA	Simultaneous thermal analysis
Y_p	Char yield, final char mass to initial char mass (%)
(MCC)	Microscale Combustion Calorimetry
pHRR	*P*eak heat release rate (W g^{-1})
T_p	Temperature of peak heat release rate (pyrolysis temperature) (°C)
HRC	Heat release capacity (J K^{-1})
THR_{MCC}	*T*otal heat release (kJ g^{-1})
Cone	Calorimetry (CC)
TTI	Time to ignition (s)
TFO	Time to flameout (s)
TTP	Time to peak heat release rate (s)
pHRR	Peak heat release rate (kW m^{-2})
THR_{CC}	Total heat release (MJ m^{-2})
TSP	Total smoke production (m^2)
MARHE	Maximum average rate of heat release (kW m^{-2})
COY	CO yield (g kg^{-1})
CO2Y	CO_2 yield (kg kg^{-1})
COP	CO production (g s^{-1})
MLR	Mass loss rate (g s^{-1} m^{-2})

2) Surface treatments usually consist of a thin layer intumescent coating (<300 μm dry film thickness), that swells upon heating to form an insulating foam, reducing the heat flux to the wood.

Both treatments target developing fires to increase the time to escape. Alternative treatments that modify fire performance are fire retardant filled glues, "pre-charring" or acetylation agents [17,18]. Effects of fire protecting treatments and mechanisms are widely reported in literature e.g. Refs. [19,20]. However, only a few studies examine flammability of fire retarded wood by treatment type [21–23]. As wood-based panels are expected to see the strongest increase in future consumption (+102% for veneer/plywood by 2050) [2], this work compares the two major commercially available fire protecting treatments for plywood.

This paper compares two approaches using commercial phosphorus-based fire retardant treatments on plywood, fulfilling requirements in European classifications (B-s1, d0), to identify any significant differences according to their fire behaviour in developing fires. A combination of thermal analysis, microscale combustion calorimetry and cone calorimetry have been used. Special care has been taken in sample preparation to ensure comparability and reflect end-use application, as the samples differ in density, fire retardant composition and loading, volume distribution, and in their combustible content. Few reports are found in the literature on intumescent coatings on wooden substrates [24–26], as their main application is the thermal protection of steel structures [27–30]. Hence, the novelty of this work lies in the direct comparison of surface and penetration treatments in end-use wood products using small- and bench-scale techniques. This required the development of a methodology for fire testing intumescent coatings on wood. To support the environmentally green choices of architects and engineers, boric acid free impregnation and melamine free, waterborne coatings were chosen for this study. This work aims to be a go-to guide for understanding flammability of commercial fire protected plywood boards in developing fires, to aid fire risk assessment in buildings.

2. Materials and methods

Three samples, prepared from two plywood boards (12 mm × 1230 mm x 1500 mm), were tested in this study. Plywood boards, specified as pine, were acquired from a commercial supplier of impregnated boards in a nontreated (*Pine*, Euroclass D-s2, d0) and treated version (*FRP*) (same batch, boric acid free, phosphorus based, Euroclass B-s1, d0). The third sample (*FRC*) was prepared by application of commercial water-based melamine-free fire-retardant intumescent coating (Teknosafe Flame Guard, Teknos, DK) on the untreated board, as specified in the technical data sheet to obtain Euroclass B-s1, d0. All the boards were conditioned in a room of 20 ± 2 °C and RH 40–50% for 14 days prior to flammability testing.

2.1. Sample preparation

From each of the two plywood boards, ten smaller pieces were cut (100 mm × 100 mm), the mass noted to calculate density ($n = 10$) and sawdust collected. The saw dust was kept in airtight containers until further testing. Additionally, from the untreated *Pine* board, five pieces (210 mm × 297 mm) were cut. Using a drawdown hand applicator (Wasag model 288, Erichsen, Germany) 400 μm wet coating was applied, dried overnight at 40 °C (Binder 9010-0001, Germany), and subsequently cut into 100 mm × 100 mm plaques. All prepared, coated samples were conditioned as described as above, mass noted, and

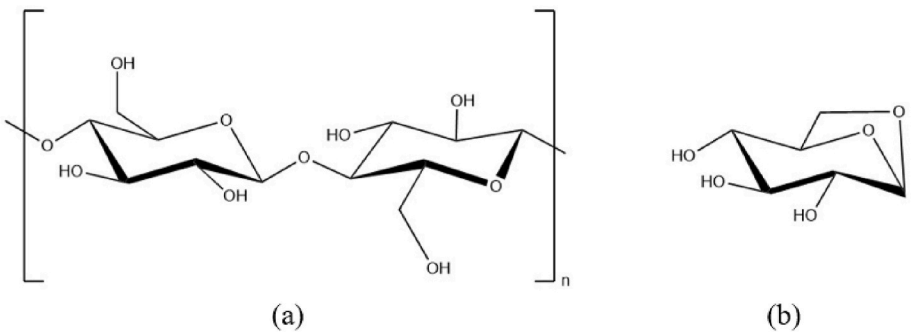

Fig. 1. Cellulose structure (a). Laevoglucosan (b).

density calculated (n = 10). Finally, dry films were fabricated by applying the coating onto PTFE film, which was then dried overnight at 40 °C. The dry films (*Coating*) were stored in zip-lock bags for further testing. Details are provided in Supporting Information (SI), section S1.

2.2. Sample characterisation

Samples were characterized by attenuated total reflectance Fourier transform infrared spectrophotometry, ATR-FTIR (iS50 fitted with iD5, ZnSe crystal, Thermo Scientific, USA) and with six area scans by scanning electron microscopy, SEM-EDAX (Quattro ESEM, ETD detector, Thermo Scientific, USA) in different regions. Dry film thickness (*DFT*) of each coating was measured (n = 5) from SEM images using ImageJ software [31]. With a pycnometer (100 mL stainless steel, TQC Sheen, NL) and a scale (Mettler Toledo, XSR105 DualRange, Switzerland), wet coating density was determined (n = 3). Solid content of the coating was determined by weighing 10.0 g paint into disposable aluminium pans (n = 3) (Ø75, 20 mm height, VWR, DK), and weighing after drying at 110 °C for 2 h.

2.3. Thermal analysis (STA)

Simultaneous thermogravimetric analysis (STA 1500, Rheometric Scientific, UK) was conducted in the temperature range 35 °C–800 °C/900 °C with a linear heating rate of 10 °C min^{-1} in nitrogen (n = 3) and in air (n = 3) at 50 cm^3 flow, with sawdust sample masses of 5 ± 0.5 mg (for dry coatings 1 ± 0.5 mg), in open platinum crucibles. As *FRC* could not realistically be represented as a sample, the fire retardant coating was tested alone without wood. Mass loss curves were differentiated and smoothed (moving average of 50 points) to localize T_{onset} and T_{max} for each mass loss step. Heat flow was measured during each run. The low sample masses of coatings result in too low signal-noise ratio in heat flow measurements to be included in the analysis.

2.4. Microscale Combustion Calorimetry (MCC)

Heat release rate was measured as a function of temperature for the dry coating (n = 6) and sawdust of *Pine* (n = 3) and *FRP* (n = 3) under pyrolysis and thermoxidative decomposition conditions on a microscale combustion calorimeter (MCC, Micro Calorimeter, Fire Testing Technology, UK) in accordance with ASTM D7309-13. Samples were weighed before and after measurements on an external balance (Mettler Toledo, XSR105 DualRange, Switzerland) and char yield Y_p calculated. Flammability parameters *pHRR*, T_p, *HRC,* and *THR* were extracted with the MCC CurveFit software following guidelines given in the FAA report [32].

2.5. Cone Calorimetry (CC)

Samples of *Pine*, *FRP,* and *FRC* were tested in quadruplicate (n = 4) on an iCone+ (Fire Testing Technology, UK) at an applied heat flux of 50 kW m^{-2} following ISO 5660–1:2015 with a sample holder (without retainer frame) fitted with insulating fibre blanket. The spark igniter was used to ignite the samples as specified in the standard. The distance between base plate of radiant heater and horizontal sample position adjusted to 25 mm, and an alternative end-of-test condition (of 2000 s) was employed. Additionally, the mass before and 2 min after the test ended was measured on an external balance (Mettler Toledo, XSR105 DualRange, Switzerland) and char yield Y_p calculated. *HRR* curves are plotted using representative data (in the middle of the range), rather than averaged data which loses some fine detail. THR curves are shown for all samples. The following parameters were extracted in accordance with ISO 5660-1: *TTI*, *TTP*, *pHRR*, *TSP*, *MARHE*, *COY,* and *CO2Y*.

3. Results

Table 1 summarizes the analytical data acquired. Coating density was 1300 ± 40 kg m^{-3} with solid content of 63 ± 1 wt%, and the applied dry film thickness was 200 ± 30 μm. Details are given in SI section S2, S3, and S4.

As expected, both fire protective treatments are phosphorus based. IR spectra, together with elemental analysis of the fire retardant coating, reveal phosphorus bands from ammonium polyphosphate (APP) and traces of inorganics: all components expected were present in intumescent fire retardant coating formulations. Functional groups ascribed to mono ammonium phosphate (MAP) were found in the IR spectrum for *FRP*. The bands in the *Pine* IR spectrum match the IR spectra reported in literature for wood [6,33]. The density differences between *Pine* and treated plywoods (*FRP* + 9.5%, *FRC* + 6.6%) are a direct measure of dry fire retardant loadings, which are not uniformly distributed over sample volume.

3.1. Microscale decomposition

Fig. 2 shows mass loss and mass loss rate as a function of temperature for *Pine*, *Coating* and *FRP* under N_2 (A) and air (B), respectively.

Fig. 2 shows that in N_2, *Pine* had a single step thermal degradation (-68%) with an onset temperature of 243 °C which left 17% residue at 800 °C. In air, char oxidation occurred after 347 °C and up to 520 °C, resulting in *Pine* char residue below 5%. *Coating* showed a stepwise thermal degradation with onset around 218 °C. In air, *Coating* mass loss reached a plateau from 360 °C to 500 °C, but with a slow mass loss after 500 °C to yield a residue of 22% (34% in N_2). It is interesting to see how closely the *Coating* follows the decomposition of *Pine*, up to 400 °C in both air and nitrogen. Presumably, the swelling of the *Coating* keeps the underlying *Pine* temperature below the decomposition onset temperature. In contrast, *FRP* decomposed around 50 °C earlier, but in doing so allowed the formation of a more resilient char. The thermal degradation of the *FRP* remained unaffected by atmosphere; an onset temperature of 174 °C for the first mass loss step (around 40%), a mass loss plateau around 50% from 300 °C to 500 °C, and char residues approaching 4% at 800 °C. (TGA data is given in SI, Table S5-1, and S5-2).

Fig. 3 shows heat flow measured in air for *Pine* and *FRP* as a function of temperature.

Fig. 3 shows a significant reduction in peak heat flow for *FRP* compared to *Pine* in the temperature interval from 300 °C to 500 °C. Even though a similar bimodular, exothermic curve shape is evident for both samples, *FRP* shows slightly earlier onset as well as a prolonged heat flow after 500 °C. In addition, a small endothermic dip around 200 °C (arrowed) is detected for *FRP*.

Fig. 4 shows heat release rate measured in MCC as a function of temperature for *Pine*, *Coating* and *FRP* under N_2 (A) and air (B), respectively.

Pyrolysis temperatures (T_p) in Fig. 4A show that *FRP* had the earliest decomposition resulting in release of volatile fuel (T_p = 276 °C). *Pine* and *FRP* show char oxidation in air above 400 °C with appearance of a second peak (Fig. 3B). Further, *FRP* displays a heat release rate of around 20 W g^{-1} above 600 °C and until end of test. Comparing pyrolysis in nitrogen and air, *Coating* (Fig. 4A and B) reveals a significant decrease in peak heat release (−33%), earlier onset of heat release rate (- 50 °C), and lower *THR* in air (5 vs. 7 kJ g^{-1}). Extracted flammability parameters from MCC are summarized in Table 2. (Remaining MCC data is found in SI, Table S6).

From Table 2 *Pine* and *FRP* had lower *THR* in N_2 than air (*Pine* 11 vs. 17 kJ g^{-1}, and *FRP* 4 vs. 10 kJ g^{-1}). Further, *FRC* demonstrates only slightly lower Y_p in air.

3.2. Bench-scale burning behaviour in well-ventilated fires

Fig. 5 shows representative *HRR* curves (A) and *THR* (B) for all

Table 1
Sample data in overview. ρ: density of plywood after conditioning. Elemental composition from SEM-EDAX, which for *FRC* is based on dried coating without substrate, since that should be identical to *Pine*.

Sample	ρ	Elements [%]				ATR-FTIR
	[kg m^{-3}]	C	O	N	P	
Pine	694 (±9)	48 (±0.2)	51 (±0.5)	1.0 (±0.3)	–	Cellulose, hemicellulose, lignin
FRC Fire Retardant Coated	740 (±19)	40 (±4)	44 (±1)	7.7 (±0.6)	6.7 (±0.6)	Ammonium polyphosphate (APP) based coating
FRP Fire Retardant Pressure impregnated	760 (±17)	47 (±2)	48 (±0.9)	3.2 (±2)	1.8 (±0.5)	Ammonium phosphate (MAP) based impregnation

(−) Below detection limit.

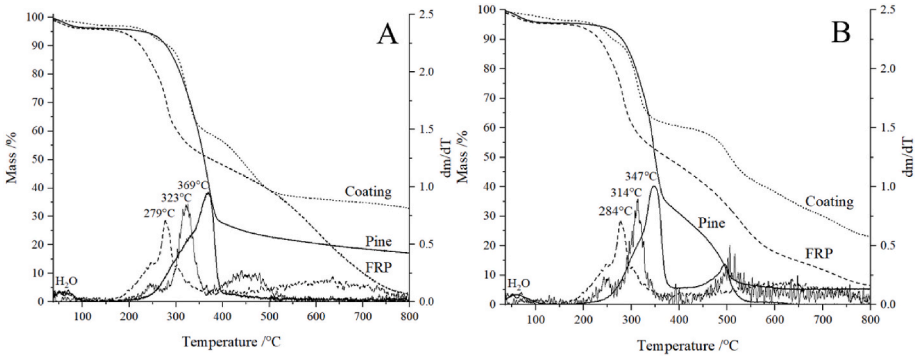

Fig. 2. Thermograms with corresponding mass loss rates (right hand axes) and T_{max} measured (A) in nitrogen and (B) in air for *Pine* (line), *FRP* (dash) and *Coating* (dot), respectively, with a scan rate of 10 °C min^{-1}. Initial mass loss below 200 °C is ascribed to water desorption.

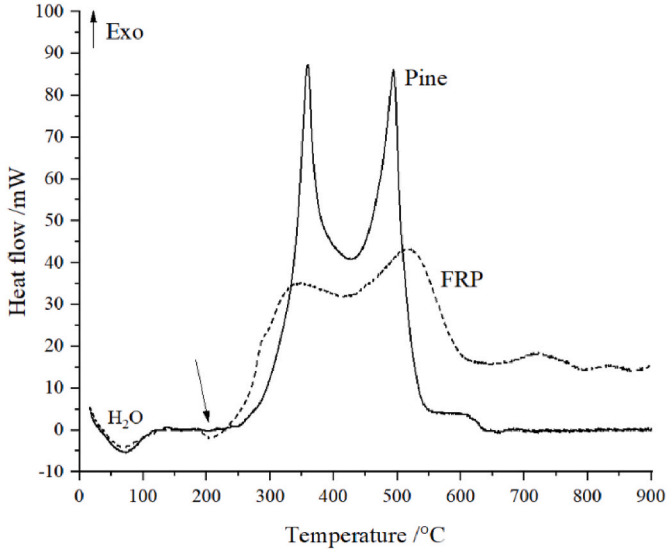

Fig. 3. Heat flow as a function of temperature measured on STA in air for *Pine* (line) and *FRP* (dash), both with sample mass 5.0 mg.

replicates as a function of time under a radiant heat flux of 50 kW m^{-2} (Replicate data is found in SI, section S7).

After the initial *HRRs* of *Pine* (220 kW m^{-2} from 10 to 100 s) and *FRC* (70 kW m^{-2} from 12 to 25 s) shown in Fig. 5A, *Pine, FRP,* and *FRC* have broadly comparable heat release rate (*HRR*) profiles. The coating layer of *FRC* expanded to generate a foam but ignited around the edges of the sample. *FRP* charred without swelling, and ignition followed as the upper plywood layers cracked and opened upwards. For all samples, increase in *HRR* after 400 s is attributed to sample warpage (towards cone heater) and increased heat exposure from burnthrough, followed by flameout and glowing combustion, around 150 s after the *HRR* peak. After flameout and until around 1500 s, *HRR* levels of *FRP* and *FRC* are significantly lower than for *Pine*. From Fig. 5B *THR* decreases in the order *Pine* > *FRC* > *FRP*, with largest standard deviation for *FRP* (±16%) compared to *FRC* and *Pine* (±4%). After flameout, *THR* curves showed slower increase corresponding to char oxidation forced under the cone heater.

Fig. 6A shows carbon monoxide production (*COP*) for *Pine*, *FRC* and *FRP*, and for *FRP*, a plot of *HRR* and specific mass loss rate (*MLR*) is shown in Fig. 6B.

Fig. 6A shows that most CO is released before ignition, or after extinction. It shows a significantly greater *COP* for *FRP* pre-ignition and post-flameout (almost double that of *Pine* or *FRC*). *Pine* and *FRC* had similar maximum *COP* values, but *FRC* shifted the maximum from 700 s to 1400 s. A linear decrease in *COP* was observed after 800 s for *Pine,* and 1500 s for *FRC* and *FRP*. Interestingly, Fig. 6B shows that the initial mass loss rate peak for *FRP* (around 100 s), does not have a corresponding *HRR* peak, but overlaps with the initial peak in *COP*. No such observations were made for *FRC* or *Pine*. Extracted parameters from CC measurements are listed in Table 3.

The main findings from Table 3 are, that both fire protective treatments significantly improve the fire performance of wood. When compared to *Pine*, *FRP* and *FRC* respectively, exhibit reduction in *THR* (-45% vs. −21%), increase of *TTI* (+468% vs. 748%), and enhanced char yield Y_p (+414% vs. + 271%). Further, *FRC* postponed *TTP* by further 31%, and reduced mean yield of CO by 55% compared to *FRP*. Since high yields of CO and smoke are associated with incomplete combustion, it is surprising that the *FRP* samples result in the lowest smoke (as *TSP*), but the highest *COY*. (Photos of post-CC chars are shown in SI, section S8).

4. Discussion

4.1. Comparison of different sample treatments

In this work special attention was given to sample preparation as wood is bought and used by volume (in m^3), impregnation loading measured as kg m^{-3} and paint applied as g m^{-2} or μm. Both treatments upgrade untreated plywood from Euroclass (D-s2, d0) to (B-s1, d0) using inorganic phosphate fire retardants (MAP and APP, Table 1). Even though these commercial timber products are used interchangeably in

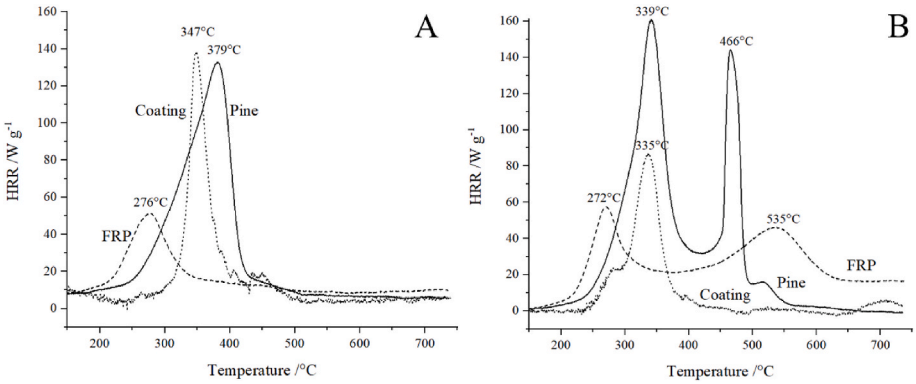

Fig. 4. Heat release rate (*HRR*) without baseline correction as function of temperature under nitrogen (A) and air (B) normalised by initial sample mass. For each local *HRR* maximum, pyrolysis temperatures (T_p) are given.

Table 2
Extracted flammability parameters from MCC. Note, temperatures at peak heat release (T_p) are given in Fig. 4 for each local maximum.

	pHRR		THR		Y_p	
	[W g^{-1}]		[kJ g^{-1}]		[%]	
	N_2	Air	N_2	Air	N_2	Air
Pine	122 (±6)	157 (±5)	11.1 (±0.3)	16.8 (±0.4)	12 (±2)	–
FRP	43 (±2)	54 (±2)	4.4 (±0.5)	9.6[a] (±0.2)	34 (±1)	7.7 (±1)
FRC	129 (±6)	87 (±5)	6.8 (±0.6)	5.4 (±0.4)	37 (±8)	29 (±7)

(–) Below detection limit.
[a] Underestimated due to baseline correction.

the construction sector, all timbers were burned, and the results normalised per gram of initial sample mass or m^2 in fire tests. Thus, *Pine* and *FRP* were made from the same plywood, from the same batch, including glue (which may be melamine formaldehyde or vinyl acetate based), but *FRP* was subject to vacuum-pressure impregnation. Coincidentally, preparation of *FRC* by paint application on *Pine*, resulted in *FRC* and *FRP* samples having approximately the same mass, thickness, and density. Thus, although testing wood samples by volume rather than mass is generally important, in the cases described here, the sample densities were sufficiently similar for the distinction to be insignificant. The methodology presented enables comparison of fire behaviour of treated timbers regardless different fire-retardant mechanism, loadings, and volume distribution. However, for samples of significantly different densities, the results should be normalised by volume rather than by mass.

4.2. Thermal decomposition

4.2.1. Pine plywood

Pine displays a single step pyrolysis from 243 °C to its maximum at 369 °C (Fig. 2A) accompanied by a peak heat release rate at 379 °C in MCC (Fig. 4A) in agreement with literature [8,18,20]. In air, the condensed phase reacts exothermically to give two sharp peaks (Fig. 3), both accompanied by release of combustible volatiles measured in MCC (Fig. 4B). A plausible explanation is that the first peak is volatilisation of laevoglucosan, leaving a dehydrated residue (char precursor) which decomposes (homolytic cleavage and condensation [12]) to produce an aromatic char. The second exothermic peak (495 °C, Fig. 3) suggests oxidation of the aromatic char with release of flammable gases (466 °C, Fig. 4A) to give an increase of *THR* of almost 6 kJ g^{-1} (Table 2) consistent with literature [11]. When the surface temperature of the plywood reaches 300–500 °C in air, mass loss (Fig. 2A) resulting in combustible volatiles (Fig. 4A), and energy release from simultaneous char oxidation (Fig. 3) were found to be at their highest, thus promoting ignition. To inhibit the ignition of wood, targeting the changes occurring over the temperature interval 300–500 °C is crucial for fire protection purposes.

4.2.2. Thermal decomposition and fire-retardant mechanisms of pressure impregnated plywood

While the initial mass loss step for *FRP* (- 50 wt%, Fig. 2) is accompanied by a heat release peak in MCC in both atmospheres, the second mass loss step (above 300 °C) only produces fuel gases when in air (Fig. 4B). Thus, in oxygen-limited atmospheres (e.g. below the flame), *FRP* provides dilutants to the flame zone, as an estimated 50% mass loss is ascribed to release of non-combustible gases. Another fire protecting mechanism of *FRP* is through promoting charring of wood, evident by

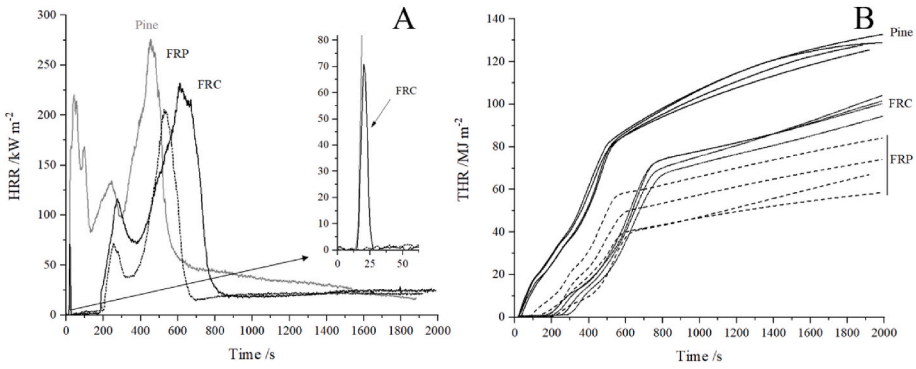

Fig. 5. (A) Heat release rate as a function of time. Representative curves for *Pine*, *FRP*, and *FRC* are shown together with an insert for the first 50 s. (B) Total heat release, shown for all replicates as a function of time.

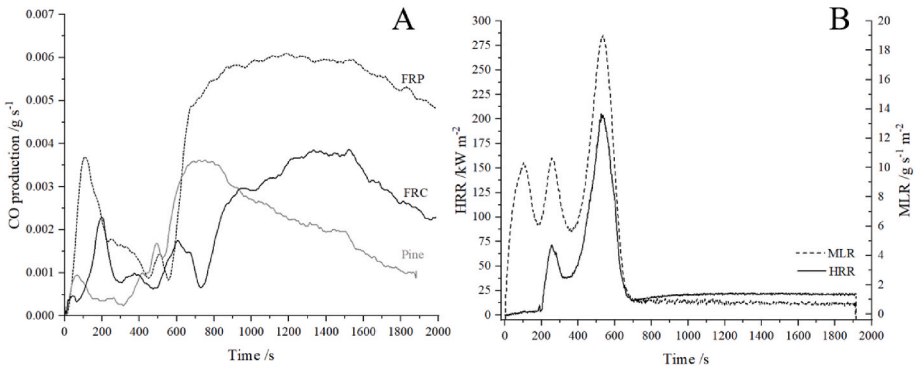

Fig. 6. (A) Carbon monoxide production (*COP*) as a function of time. Representative curves of *Pine*, *FRC*, and *FRP* are shown. (B) Heat release rate plotted together with specific mass loss rate of *FRP*.

Table 3
CC results for the entire test period of 2000 s. For comparison of treatments mean and standard deviation of initial sample masses were *Pine* 86 g ± 1 g, *FRC* 90 g ± 2 g, and *FRP* 91 g ± 2 g.

	TTI	TTP	pHRR	THR	TSP	MARHE	Y_p	COY	CO2Y
	[s]	[s]	[kW m^{-2}]	[MJ m^{-2}]	[m^2]	[kW m^{-2}]	[%]	[g kg^{-1}]	[kg kg^{-1}]
Pine	25 ± 8	424 ± 3[b]	280 ± 19	127 ± 4	3.5 ± 0.4	165 ± 14	3 ± 0.5	47 ± 4	1.32 ± 0.019
FRP	142 ± 5	491 ± 41	186 ± 28	70 ± 11	2.4 ± 0.6	79 ± 18	17 ± 1	138 ± 10	0.92 ± 0.07
FRC	212 ± 58[a]	642 ± 24	223 ± 20	100 ± 4	4.8 ± 0.3	92 ± 6	13 ± 1	62 ± 3	1.10 ± 0.025

[a] Ignition occurred around 20 ± 5 s (see Fig. 4A) but not sustained flaming whereby *TTI* is reported as time to recognition. The spark igniter was not removed until sustained flaming was observed.

[b] *TTP* was detected around 38 s for two of four *Pine* samples. For comparison, *TTP* for *Pine* is reported as an average ($n = 2$) when peak heat release was detected on the second peak.

earlier decomposition in both atmospheres (between 50 and 70 °C lower, Figs. 2, and Fig. 4). This is supported by an endothermic dip in Fig. 3 indicating phosphorylation and release of phosphoric acid catalysing dehydration and crosslinking of char precursors [20,34]. Condensed phase fire retardants (such as MAP) are well-known for their ability to promote char formation by favouring dehydration by reaction with C-6 hydroxyl groups on cellulose [7,35]. Lastly, Fig. 3 shows reduced exothermal heat flow of *FRP* from 300 to 500 °C compared to *Pine*. Together with low measured *HRR* from released volatiles (20–25 W g^{-1}, Fig. 4B), this suppresses ignition. However, above 600 °C *FRP* undergoes exothermic reactions (Fig. 3) that continuously feed combustible gases to the fire (Fig. 4B) indicating a significant char oxidation process. From 600 °C to 800 °C, a highly cross-linked, aromatic char is reported to degrade and release low-molecular weight species such as acetylene, and CO_2 [11,12]. Hence, the pressure impregnated phosphorus delays the energy release. Altogether, these three fire-retardant mechanisms are revealed for *FRP* by combination of STA and MCC.

4.2.3. Thermal decomposition and fire-retardant mechanisms of coating

An initial mass loss rate peak (218–250 °C, Fig. 2) is evident in both atmospheres which is not accompanied by a fuel release in air (Fig. 4B). This is ascribed to the intumescent reaction, where APP condenses with the polyol or cellulose to release NH_3 and H2O [36,37]. Not surprisingly, the coating forms a char barrier before 300 °C. A second mass loss of 30% (300–400 °C, Fig. 1) overlaps with *Pine* to give heat release from combustible gases (Fig. 4), possibly originating from the binder. This suggests that early char formation is a prerequisite for intumescent fire protection of wood. Once the char is established, no further heat release is evident after 450 °C, despite an observed mass loss from 500 °C in air. This is proposed to result from depolymerisation of the APP chain above 500 °C with release of P_2O_5 or non-combustible phosphate-carbon compounds [38]. It is also possible that release of phosphorus compounds to the gas phase could inhibit flaming combustion [39]. Altogether, an intumescent coating works by the barrier effect, and after swelling and charring, a high thermoxidative resistance of the layer is observed.

4.2.4. Comparison of TGA and MCC data

Comparing the shape of the mass loss rate curves from TGA (Fig. 2) in nitrogen with those of MCC (Fig. 4), where only the loss of combustible volatiles is recorded, it is clear that while volatiles from *Pine* are combustible, less than a third of the volatiles from *FRP* are combustible at 900 °C in the MCC furnace, and around half of the volatiles from *FRC* are combustible. Similar behaviour was observed in the cone calorimeter (Fig. 6B) where the first mass loss peak had no corresponding *HRR* peak.

In air, while *Pine* shows a sharper second peak in MCC than TGA (despite the faster heating rate in MCC), the peak shapes are similar [40]. *FRP* shows a much smaller peak than *Pine* in MCC at 272 °C, indicating less combustible release, but a stronger peak at 535 °C. *Coating* also shows a delayed and smaller peak in MCC than TGA.

4.3. Characterisation of fire behaviour

Both fire protective treatments reduce total heat release (by 21% for *FRC*, and by 47% for *FRP* from Fig. 5B), promote char formation, and inhibit glowing combustion by a reduced heat release rate after flameout (700 s–1500 s, Fig. 5A). The presence of phosphorus is known for these effects [7]. While ranking of samples according to *THR* is tempting, in this work *THR* is measured after 2000 s. Even though this is close to conventional end conditions of ISO 5660, non-flaming char oxidation masks *THR* comparison. Thus, impacts from promotion of char by fire retardants at the expense of flammable volatiles during developing fires, are easily missed when comparing values in Table 3. Nevertheless, with a similar loading of phosphorus (ρ, Table 1) distributed in the wood bulk, *FRP* shows both superior *THR, MARHE* and Y_p compared to *FRC* (Table 3). Further, *FRP* shows significant increase of CO production in the entire test period (Fig. 6A) accompanied by constant *MLR* after flameout (Fig. 6B), but without rise in total smoke production (*TSP*,

Table 3). As the main heat release step in combustion is the conversion of CO to CO_2, any reduction in this process will lower the *HRR*. This is especially true for the pre- and post-flaming fire stages. By calculation of the CO/CO_2 ratio, an indicator for the degree of incomplete combustion, 0.15 is obtained *FRP* (i.e. COY/CO2Y, Table 3). This is 3–5 times higher than for *Pine* and *FRC* (0.03 and 0.05). For comparison, under-ventilated flaming combustion of wood has CO/CO_2 around 0.24 [41,42]. The higher CO/CO_2 ratio may result from more effective gas-phase quenching of flaming combustion by the penetrative treatment (favouring CO over CO_2) or greater char oxidation from the residue of the *FRP*. Combined with the shifted and prolonged energy release pattern discussed in section 4.2.2, char oxidation is suggested as the main cause of the significant CO production. Altogether, the impregnation treatment minimises fuel gas release, enhances char formation and increases CO yields.

From heat release curves in Fig. 5A, *FRC* exhibited a short flash of flaming around 20 s (Fig. 5A, insert). Thermal analysis indicates early binder decomposition, which fuelled this flash. The release of combustible volatiles is limited by fast char expansion, which suppresses sustained flaming until *TTI* around 212 s (Table 3). In addition, detection of time to peak heat release and burnthrough for *FRC* is delayed by more than 150 s compared to *FRP* (Table 3), an effect not reported before. The delay in *TTP* is suggested as a measure of the barrier heat insulation property [43,44]. By slower sample temperature rise, a slow-down of decomposition and fuel gas release is expected, which in turns delays burnthrough by almost 150 s. Curiously, of all samples *FRC* had the highest total smoke production (4.8 m^2, Table 3), also found in other fire scenarios [43]. This is further supported by thermal analysis (section 4.2.3). With an apparent *THR* reduction of *FRP* of - 21%, and char yield enhancement by a factor 4 compared to *Pine*, the fire performance is mainly dictated by the barrier effect.

4.3.1. Behaviour during the flaming phase

For this work, it is important to separate the flaming fire stage, where the additional heat flux from the flame drives fire growth, from the post-flaming fire stage. The post-flaming, char oxidation stage, driven by the 50 kW m^{-2} heat flux from the cone heater can be disregarded as a factor driving fire growth, but is of critical importance in terms of smoke toxicity and structural failure. Thus, a selection of the data originally shown in Table 3 has been recalculated for the period up to flameout and is presented in Table 4. Time to flameout (*TFO*) was identified for each dataset as the inflection point of the *THR* curve in Fig. 5B.

Table 4 shows significantly lower *THR* for the flaming phase than for the entire test particularly for *FRP* and *FRC*. However, the data also show correspondingly greater char residues, which, if expressed as a ratio of *THR* to mass lost, do not differ significantly from the same data for the whole test showing that the calorific value of the volatile fuel is unaffected by the presence of a flame. Thus, the reason for the lower heat release during the burning stage is the smaller mass loss.

From Table 3, both *FRP* and *FRC* exhibit significant reduction in *pHRR* (34% vs. 20%) and delay *TTI* (142 s vs. 212 s). In the fire protection of timber, the principal objective is to limit fire spread. Fire spread over a surface is dependent on the material's ignitability. However, it is also argued that *pHRR* is the single most important factor dictating fire growth. The relative importance of these two factors (surface spread of flame and flame penetrating into the bulk of the material) depends on the material burning, the geometry and the fire scenario. Thus, the crucial data affecting fire growth are *TTI* and *pHRR*. However, it is questionable whether the initial peak for *FRC* is sufficient to promote fire growth. In addition, *pHRR* is detected on the last peak corresponding to sample distortion, increased reradiation from the aluminium backing and burnthrough. Thus, to avoid artefacts of the testing method, differences in behaviour of the three materials during developing fires are best understood by *HRR* curves given in Fig. 5A up to 400 s. For *Pine*, the appearance of smaller bursts of heat release in the *HRR* curve were observed to correspond to the burning of separate plywood layers. While *Pine* shows an *HRR* peak reaching 220 kW m^{-2} from 10 to 150 s, *FRP* and *FRC* effectively suppress ignition and prevent release of flammable gases for around 142 s and 212 s, respectively, and lower *pHRR* to around 120 kW m^{-2} for both (119 ± 41 kW m^{-2} vs. 122 ± 12 kW m^{-2}, SI section S8). This shows the extent to which both *FRP* and *FRC* can withstand the large thermal attack of 50 kW m^{-2}. In comparison, the maximum heat flux in the EN 13823 single burning item test is around 44 kW m^{-2} [45].

Table 4
THR and Y_p from cone calorimetry from 0 s to flameout.

	TFO	THR	Y_p
	[s]	[MJ m^{-2}]	[%]
Pine	520 ± 9	81 ± 1	23 ± 2
FRP	592 ± 31	46 ± 9	34 ± 3
FRC	757 ± 19	69 ± 3	39 ± 9

4.4. Contribution to fire

4.4.1. Pine plywood

During oxidative thermal decomposition in STA and under the cone heater *Pine* yields a char residue of 3–4%. Thus, the maximum combustible content of plywood is estimated to be around 96% by mass with a total heat release of 15–17 kJ g^{-1} according to oxygen depletion measurements (THR_{CC} = 15.3 kJ g^{-1}, THR_{MCC} = 16.8 kJ g^{-1}). This is found to be in good agreement with literature, that reports calorific values from bomb calorimetry of 18–19 kJ g^{-1} for pine [18]. This shows that the process of turning virgin wood into plywood did not have a significant effect on the fuel content. The main pyrolysis of *Pine* takes place between 300 °C and 500 °C. Fire behaviour measured by exposure to 50 kW m^{-2} shows *TTI* around 20 s and *pHRR* values around 220 kW m^{-2}, similar to results reported elsewhere [13,40,46,47].

4.4.2. Pressure impregnated plywood

Thermal analysis in air revealed a char yield of 7%–8%. Thus, the maximum combustible release from *FRP* was 93% in MCC, but 83% in CC by mass, with a total heat release according to oxygen depletion measurements of 7–9 kJ g^{-1} (THR_{CC} = 7.7 kJ g^{-1}, THR_{MCC} = 9.6 kJ g^{-1}). With a density increase corresponding to 9.5% addition of fire retardant by dry mass, a total heat release reduction of 47–53% was obtained. Hence, contribution to fire is significantly reduced by pressure impregnation. Impregnated wood had multiple fire retardation mechanisms: release of non-combustible volatiles; accelerated char formation; delay in energy release profile as a consequence of greater char stability; and the inhibition of the main heat release step, converting CO to CO_2, particularly in the non-flaming stages. Acceleration of charring resulted in less liberation of flammable volatiles in the stages critical for flaming combustion of pine (around 300 °C–500 °C) which in cone calorimetry resulted in significant improvement in *TTI* (+468%), even though combustible gases and CO are continuously released over a wide temperature range, in particular during the smouldering phase.

4.4.3. Coated plywood

The maximum volatile content of the coating alone is evaluated to be around 70% (Y_p 22–29% in air) obtaining THR_{MCC} = 5.6 kJ g^{-1}. When applied on *Pine* substrate, *FRC* is evaluated to have a maximum combustible content of around 94% (as the weighted average of *Pine* and *FRC*) with a measured THR_{CC} of 11.1 kJ g^{-1}. Hence, the total heat release is reduced by 26–34%. With a density increase of 6.6% corresponding to the loading of fire retardant by dry mass, the total heat release reduction is within the same order of magnitude as for *FRP*. By experimental design, the amount of coating seems to be the limiting factor for fire performance of coated plywood. The intumescent coating showed an early flash of flaming, but by swift expansion, the charring foam decreased the mass transport of flammable volatiles, extinguishing

the early flame. Further, the char was found to limit the substrate temperature increase and delay burnthrough measured as *TTP*. The char layer acted as an oxidation shield, but increased smoke obscuration. This is suggested to be APP decomposition, an effect not understood in detail.

It is important to note the severity of the methodology used for *FRC* in cone calorimeter testing. In normal use, the coating would cover all exposed surfaces, and provide fire protection to them. In this case, the coated samples were cut, leaving the unprotected sample sides exposed. Observation showed that flaming started at these unprotected sides. Although the sample sides could have been coated, or the upper sample retaining frame used, this would also have been unrepresentative of the end-use scenario. It is an inherent limitation of the cone calorimeter methodology for assessment of fire protective coatings. In addition, it is important to note that the swollen layer would be subject to a greater applied heat than the *FRP* sample, because of the proximity of the swollen foam to the cone heater. Again, this is an artefact of cone calorimeter testing of intumescent materials, which would not occur in a large-scale fire.

5. Conclusions

Phosphorus-based fire protective surface and penetration treatments are demonstrated to be highly effective in reducing the flammability of timber. By micro- and bench-scale oxygen depletion calorimetry, untreated plywood showed total heat release of 15–17 kJ g^{-1}, coated plywood around 11 kJ g^{-1} and pressure impregnated timber had the best performance with 7–9 kJ g^{-1}. Even though a simple ranking is possible, and both treated timbers hold a Euroclass B-s1, d0 classification, understanding the nature of their different flammability is critical for fire safety. With STA and MCC, impregnated timber showed an earlier onset of dehydration that accelerated char formation, increased the char decomposition temperature, and increased the CO yield. CO release reduces heat output but contributes to the toxic hazard. Char expansion of the intumescent coating postponed sustained flaming by barrier formation, limiting combustible volatile release which delayed burnthrough, however increased smoke production. Compared to the impregnated treatment, which was fire protected throughout its bulk, the coating only provided fire protection to the uppermost surface in cone calorimetry, and was subjected to a greater applied heat flux as the result of swelling towards the cone heater.

All these effects are crucial in fire risk assessment of construction materials targeting developing fires. Even though this work demonstrated high convenience of cone calorimetry to include surface coated wood products, it also discusses how to process and interpret cone data when multiple fire stages are present.

CRediT

I. Hansen-Bruhn: Conceptualization, Formal analysis, Investigation, Methodology, Validation, Visualization, Writing - Original Draft, Writing - Review & Editing. T.R. Hull: Conceptualization, Formal analysis, Resources, Project administration, Supervision, Writing - Review & Editing.

Declaration of competing interest

The authors declare that they have no known competing financial interests or personal relationships that could have appeared to influence the work reported in this paper.

Data availability

All data are provided in the Supplementary Material

Acknowledgements

This work was supported by Innovation Fund Denmark [grant no 9065-00233B]. The authors thank Clare Bedford, and Kirsten Jensen for help with data acquisition.

Appendix A. Supplementary data

Supplementary data to this article can be found online at https://doi.org/10.1016/j.firesaf.2023.103918.

References

[1] Food and Agriculture Organization of United Nations, Forestry Product and Trade Data, Faostat, https://www.fao.org/faostat/en/#data/FO (accessed on May 30, 2023).
[2] Food and Agriculture Organization of United Nations, Global Forest Section Outlook 2050, Assessing Future Demand and Sources of Timber for a Sustainable Economy, 2022. https://www.fao.org/3/cc2265en/cc2265en.pdf. (Accessed 30 May 2023).
[3] UK Parliament 2023, The Environmental Audit Committee, Press release, 25 July 2022, https://committees.parliament.uk/work/6880/sustainable-timber-and-deforestation/news/172336/what-impact-will-increased-timber-use-in-the-future-have-on-global-deforestation/. (Accessed 10 June 2023).
[4] World Bank. https://www.worldbank.org/en/topic/forests/forests-area#1. (Accessed 31 May 2023).
[5] World Bank, World Bank Group Forest Action Plan PY16-20, 2016. https://documents1.worldbank.org/curated/en/240231467291388831/pdf/106467-REVISED-v1-PUBLIC.pdf. (Accessed 31 May 2023).
[6] H. Yang, R. Yan, H. Chen, D.H. Lee, C. Zheng, Characteristics of hemicellulose, cellulose and lignin pyrolysis, Fuel 86 (12–13) (2007) 1781–1788.
[7] D. Drysdale, An Introduction to Fire Dynamics, John Wiley & Sons, 2011.
[8] T. Hirata, S. Kawamoto, T. Nishimoto, Thermogravimetry of wood treated with water-insoluble retardants and a proposal for development of fire-retardant wood materials, Fire Mater. 15 (1) (1991) 27–36.
[9] F. Shafizadeh, A.G.W. Bradbury, Thermal degradation of cellulose in air and nitrogen at low temperatures, J. Appl. Polym. Sci. 23 (5) (1979) 1431–1442.
[10] J. Alongi, G. Malucelli, Thermal degradation of cellulose and cellulosic substrates, React. Mech. Therm. Ana. Adv. Mater. 14 (2015) 301–332.
[11] D. Price, A.R. Horrocks, M. Akalin, A.A. Faroq, Influence of flame retardants on the mechanism of pyrolysis of cotton (cellulose) fabrics in air, J. Anal. Appl. Pyrol. 40 (1997) 511–524.
[12] F. Shafizadeh, Y. Sekiguchi, Development of aromaticity in cellulosic chars, Carbon 21 (5) (1983) 511–516.
[13] L.A. Lowden, T.R. Hull, Flammability behaviour of wood and a review of the methods for its reduction, Fire Sci. Rev. 2 (2013) 1–19.
[14] A.J. Stamm, Thermal degradation of wood and cellulose, Ind. Eng. Chem. 48 (3) (1956) 413–417.
[15] S. Soares, G. Camino, S. Levchik, Comparative study of the thermal decomposition of pure cellulose and pulp paper, Polym. Degrad. Stabil. 49 (2) (1995) 275–283.
[16] Construction products Europe, construction products regulation. https://www.construction-products.eu/publications/cpr/. (Accessed 30 May 2023).
[17] C.M. Popescu, A. Pfriem, Treatments and modification to improve the reaction to fire of wood and wood based products—an overview, Fire Mater. 44 (1) (2020) 100–111.
[18] R.A. Mensah, L. Jiang, J.S. Renner, Q. Xu, Characterisation of the fire behaviour of wood: from pyrolysis to fire retardant mechanisms, J. Therm. Anal. Calorim. (2022) 1–16.
[19] S.L. LeVan, J.E. Winandy, Effects of fire retardant treatments on wood strength: a review, Wood Fiber Sci. (1990) 113–131.
[20] M. Gao, C. Sun, K. Zhu, Thermal degradation of wood treated with guanidine compounds in air: flammability study, J. Therm. Anal. Calorim. 75 (2004) 221–232.
[21] B.A.L. Östman, L.D. Tsantaridis, Heat release and classification of fire retardant wood products, Fire Mater. 19 (6) (1995) 253–258.
[22] B.H. Lee, H.S. Kim, S. Kim, H.J. Kim, B. Lee, Y. Deng, J. Luo, Evaluating the flammability of wood-based panels and gypsum particleboard using a cone calorimeter, Construct. Build. Mater. 25 (7) (2011) 3044–3050.
[23] O. Grexa, H. Lübke, Flammability parameters of wood tested on a cone calorimeter, Polym. Degrad. Stabil. 74 (3) (2001) 427–432.
[24] A. Aqlibous, S. Tretsiakova-McNally, T. Fateh, Waterborne intumescent coatings containing industrial and bio-fillers for fire protection of timber materials, Polymers 12 (4) (2020) 757.
[25] A. Lucherini, Q.S. Razzaque, C. Maluk, Exploring the fire behaviour of thin intumescent coatings used on timber, Fire Saf. J. 109 (2019), 102887.
[26] C.S. Chuang, K.C. Tsai, M.K. Wang, C.C. Ou, C.H. Ko, I.L. Shiau, Effects of intumescent formulation for acrylic-based coating on flame-retardancy of painted red lauan (Parashorea spp.) thin plywood, Wood Sci. Technol. 42 (2008) 593–607.
[27] T. Mariappan, Recent developments of intumescent fire protection coatings for structural steel: a review, J. Fire Sci. 34 (2) (2016) 120–163.
[28] B.K. Cirpici, Y.C. Wang, B. Rogers, Assessment of the thermal conductivity of intumescent coatings in fire, Fire Saf. J. 81 (2016) 74–84.

[29] D. de Silva, A. Bilotta, E. Nigro, Approach for modelling thermal properties of intumescent coating applied on steel members, Fire Saf. J. 116 (2020), 103200.
[30] D. Häßler, S. Hothan, Performance of intumescent fire protection coatings applied to structural steel tension members with circular solid and hollow sections, Fire Saf. J. 131 (2022), 103605.
[31] W.S. Rasband, ImageJ, U. S. National Institutes of Health, Bethesda, Maryland, USA, 1997-2018. https://imagej.nih.gov/ij/.
[32] Federal Aviation Administration, Report No. DOT/FAA/TC-12/53, Principle and Practices of Microscale Combustion Calorimetry, 2013. https://www.fire.tc.faa.gov/pdf/tc-12-53.pdf. (Accessed 30 May 2023).
[33] J. Zhao, W. Xiuwen, J. Hu, Q. Liu, D. Shen, R. Xiao, Thermal degradation of softwood lignin and hardwood lignin by TG-FTIR and Py-GC/MS, Polym. Degrad. Stabil. 108 (2014) 133–138.
[34] G. Camino, L. Costa, Performance and mechanisms of fire retardants in polymers—a review, Polym. Degrad. Stabil. 20 (3–4) (1988) 271–294.
[35] C. Di Blasi, C. Branca, A. Galgano, Effects of diammonium phosphate on the yields and composition of products from wood pyrolysis, Ind. Eng. Chem. Res. 46 (2) (2007) 430–438.
[36] S. Duquesne, S. Magnet, C. Jama, R. Delobel, Intumescent paints: fire protective coatings for metallic substrates, Surf. Coating. Technol. 180 (2004) 302–307.
[37] I. Hansen-Bruhn, K. Jensen, J.B. Ravnsbæk, M. Hinge, Micro combustion calorimeter for development of fire protective paints, J. Therm. Anal. Calorim. 148 (10) (2023) 3993–4000.
[38] P.J. Davies, A.R. Horrocks, A. Alderson, The sensitisation of thermal decomposition of ammonium polyphosphate by selected metal ions and their potential for improved cotton fabric flame retardancy, Polym. Degrad. Stabil. 88 (1) (2005) 114–122.
[39] N. Bouvet, G. Linteris, V. Babushok, F. Takahashi, V. Katta, R. Krämer, Experimental and numerical investigation of the gas-phase effectiveness of phosphorus compounds, Fire Mater. 40 (5) (2016) 683–696.
[40] J.S. Renner, R.A. Mensah, L. Jiang, Q. Xu, A critical assessment of the fire properties of different wood species and bark from small-and bench-scale fire experiments, J. Therm. Anal. Calorim. (2022) 1–12.
[41] P. Blomqvist, T. Hertzberg, H. Tuovinen, K. Arrhenius, L. Rosell, Detailed determination of smoke gas contents using a small-scale controlled equivalence ratio tube furnace method, Fire Mater. 31 (8) (2007) 495–521.
[42] I. Hansen-Bruhn, T.R. Hull, Smoke Toxicity of Fire Protecting Timber Treatments, 2023 [In press – accepted for IAFSS 2023, and manuscript submitted to special IAFSS 2023 edition of Journal of Fire Sciences].
[43] R.M. Nussbaum, The effect of low concentration fire retardant impregnations on wood charring rate and char yield, J. Fire Sci. 6 (4) (1988) 290–307.
[44] E. Sanned, R.A. Mensah, M. Försth, O. Das, The curious case of the second/end peak in the heat release rate of wood: a cone calorimeter investigation, Fire Mater 47 (2022) 498–513.
[45] D. Zeinali, S. Verstockt, T. Beji, G. Maragkos, J. Degroote, B. Merci, Experimental study of corner fires—Part I: inert panel tests, Combust. Flame 189 (2018) 472–490.
[46] A.Y. Snegirev, Generalized approach to model pyrolysis of flammable materials, Thermochim. Acta 590 (2014) 242–250.
[47] M. Delichatsios, B. Paroz, A. Bhargava, Flammability properties for charring materials, Fire Saf. J. 38 (3) (2003) 219–228.